Contents lists available at ScienceDirect

Construction and Building Materials

journal homepage: www.elsevier.com/locate/conbuildmat

Organic-inorganic hybrid sol–gel membranes for pH sensing in highly alkaline environment

Bárbara Ferreira [a], Sara Sousa [a], Rui P.C.L. Sousa [a], Susana P.G. Costa [a], M. Manuela M. Raposo [a], Pier Parpot [a], Artur J.M. Valente [b], Rui F.P. Pereira [a,*], Rita B. Figueira [a,*]

[a] Centre of Chemistry, University of Minho, Campus de Gualtar, 4710-057 Braga, Portugal
[b] Centre of Chemistry, University of Coimbra, Department of Chemistry, Coimbra 3004-535, Portugal

ABSTRACT

This work reports the synthesis of organic–inorganic hybrid (OIH) membranes for potential optical fibre sensors (OFS) functionalisation for pH monitoring of concrete and reinforced concrete structures (RCS). As precursors, 3-glycidyloxypropyltrimethoxysilane and Jeffamine® THF-170 were used. The OIH sol–gel materials were doped with phenolphthalein (phph) for pH sensing proposes and cetyl trimethyl ammonium bromide as surfactant.

OIH membranes with pH sensing ability properties were successfully obtained. The dielectric properties of the resultant membranes were determined by electrochemical impedance spectroscopy. The logarithm of resistance obtained was 10.19 Ω cm^2 for the undoped matrix and, 7.06 Ω cm^2 for the doped one with phph. The results obtained in simulated concrete pore solutions, for the OIH produced, showed to be promising for application in fresh concrete. The transmittance of the synthesized OIH materials decreased after the doping with phph. The matrix showed intrinsic fluorescence and doping it only led to small deviations in the wavelength of the peak of maximum emission. Regarding thermal analysis, no significant changes were obtained on the thermal profile of the doped and undoped OIH membranes. The pH variation was detected by the OIH membrane colour change. Stability studies regarding the release of phph from the OIH matrix led to a mean dissolution time equal to 75.4 ($\pm$0.02) hours, indicating that the proposed system reveals long-term stability.

1. Introduction

Concrete is one of the most common used materials in the construction field due to its properties such as mechanical strength and moulding abilities. However, in certain conditions, concrete is prone to degradation namely due to the combination of physicochemical properties and the environment to which it is exposed [1]. Regarding reinforced concrete structures (RCS), it is widely accepted that the steel is protected by the concrete through a physical barrier and by the formation of a passivation film on the steel surface as a result of the high alkalinity of the concrete [2]. The high pH values, generally above 12.5, arise from the presence of calcium hydroxide (Ca(OH)$_2$) and potassium hydroxide (KOH) [1,3].

Regarding the structural concrete degradation, corrosion reinforcement and concrete carbonation are the two main phenomena that more frequently affect civil engineering structures. The concrete carbonation starts on the concrete surface and progresses to high depth, reaching the reinforcement. This phenomenon occurs due to the chemical reaction of the alkaline components of cement with atmospheric CO$_2$. As a consequence, the concrete pH falls to values between 9 and 6 and the concrete loses the ability to protect the steel rebar [4–7]. Moreover, after concrete carbonation and, in the presence of oxygen and moisture, the ideal conditions for steel corrosion onset are established [7]. The continuous evolution of RCS corrosion leads to steel ductility and, reduction of the steel reinforcement section, which in extreme situations reflects on the stability of the structure and may lead to its collapse [3,8].

Considering all the above, it is quite understandable that the development of sensors for continuous monitoring of concrete and RCS is necessary. This allows a more rational approach regarding repairing interventions and increases the service life of civil engineering structures, mitigating at the same time unpredictable costs. Monitoring parameters such as the presence of cracks [9], weathering effects [10], deformation [11], pressure [12], pH [13], humidity [14], chloride ions penetration [15] or temperature [16] help to identify the source and the

level of damage [17], and prevent earlier failure. Several electrochemical [1,17–20] and optical fibre sensors (OFS) have been developed [21–25]. Electrochemical techniques, when applied correctly, allow the acquisition of fast, quantitative, and reliable information. However, most of the electrochemical sensors reported show some shortcomings such as durability, sensitivity to electromagnetic interference and low stability over time [1]. OFS show the advantages of having reduced size, low weight, immunity to electromagnetic interference, versatility in geometry, sensitivity, and the ability to be distributed at several locations of a metallic, or a concrete structure, allowing a more detailed structural characterization. Additionally, OFS can be integrated into a wireless sensor network to be used as early warning system in critical situations. In this context, the OFS were the target of fast development [1] and in the last twenty years, several manuscripts focused on OFS for monitoring the pH of concrete structures have been reported. For instance, Grahn *et al.* [26] developed an OFS system for measuring pH in concrete, immobilizing vinylsulfonyl azo dye, diazonium salt and remasol dye as pH indicators in a polyvinylalcohol matrix. The pH variation was indicated by the colour dye/polymer system change. The sensor system exhibited long-term stability. Basheer *et al.* [27] reported the potential of OFS development, functionalized with sol–gel films, to monitor the pH condition of concrete structures. Nevertheless, the authors concluded that further experiments were needed to establish its long-term viability. In that same year, Xie *et al.* [28] described the development of an OFS to estimate the lifetime of RCS. The system was obtained through the sol–gel method using tetraethylorthosilicate (TEOS) as a precursor and cresol red as an indicator dye. McPolin *et al.* [29] developed a pH OFS to assess the carbonation occurring in cementitious materials. TEOS was used as a precursor and cresol red as an indicator dye. The authors reported that the OFS functioned properly for >18 months after placement *in situ*. Later, Nguyen *et al.* [13] developed an OFS to detect pH between 10 and 13. The reported sensor induced a change in fluorescence intensity of a coumarin imidazole dye which was covalently attached to a polymer network that was fixed to the distal end of the optical fibre. It was concluded that the developed OFS was suitable for long term monitoring of pH. In 2016, Islam *et al.* [30] reported the development of different types of sol–gel matrices doped with phenolphthalein (phph). The prepared titania and silica–titania matrices showed a stable thermal behaviour and a strong connection between the matrix and the phph [30]. Also in 2016, an evanescent wave pH OFS was fabricated through the encapsulation of different indicator dyes within the same organic–inorganic hybrid (OIH) matrix which was obtained by the sol–gel method using as precursors TEOS and titanium tetraisopropoxide in the presence of cetyl trimethyl ammonium bromide (CTAB) [31]. The dyes used were bromophenol blue, phenol red, cresol red and phph. The reported OFS showed high stability, reproducibility, repeatability, fast response and long-lasting behaviour [31]. Subsequently, an OFS functionalized with a sol–gel film for a pH range between 2 and 12 was reported [32]. The precursors used were TEOS and it was concluded that the presence of phph species in the silica matrix affected the condensation degree and the amount of water absorbed in the silica network [32]. In 2019, Grengg *et al.* [33] showed an innovative method for measuring pH in concrete that applies sensor foils based on luminescent, pH sensitive dyes for quantification and imaging of the spatial distribution of surface pH of concrete (*i.e.*, 9.35 – 12.35). The dye used was aza-BODIPY and Egyptian blue was used as a reference. Inserra *et al.* [34] developed a silica sensor to assess the pH changes in concrete in a range between 10 and 12 using the sol–gel method. The optical pH sensor showed a high sensitivity, good reproducibility and reversibility, a fast response and long-term stability. Bartelmess *et al.* [35] optimized a sensor to monitor the pH changes in the concrete. A hydrogel matrix, doped with thymus blue, whose transition point was determined to be around 11.6 was used. After concreting, the samples remained in a wooden casing for hardening. The sensor's long-term stability has been demonstrated for at least three months [35].

Following the work developed until now [36,37], in which amino-alcohol based OIH sol–gel films were reported and assessed in mortars and considering the promising results obtained for this purpose, herein is reported, for the first time, the synthesis of OIHs in which 3-glycidoxipropyltrimethoxysilane (GPTMS) and Jeffamine THF170 were used as precursors and doped with phph, to obtain pH sensing films to monitor concrete pH variations. CTAB surfactant was also introduced in the matrix since it plays an important role as pore formation agent and structure direction guide [38,39]. The use of phph as pH sensing molecule in the prepared OIH system has several advantages such as reversibility when the detection region comes into contact with an aqueous solution or with acidic or basic volatile compounds [32]. In addition, phph has been widely used for monitoring carbonation in concrete structures [40]. One of the most cited methods for this purpose in the literature is based on spraying this indicator on the surface of concrete structures. This method, which depends on pH variations, has some limitations. Besides being an *in situ* method, it is only useful for the determination of carbonation at an early stage, at the concrete surface, because in deeper areas of the structure where carbon dioxide acts, it is not possible to determine whether carbonation has actually occurred or the stage phase [41,42]. As far as the authors' knowledge, the obtained OIH sol–gel materials doped with phph and resistant to high alkaline environment herein described have never been reported.

2. Experimental section

2.1. Materials and simulated concrete pore solution

Commercial reagents 3-glycidoxipropyltrimethoxysilane (GPTMS, 97 %, Sigma-Aldrich, St. Louis, MO, USA) and Jeffamine® THF-170 (Huntsman Corporation, Pamplona, Spain), cetyl trimethyl ammonium bromide (CTAB, ACROS Organics, Antwerp, Belgium), phenolphthalein (phph, Merck, Darmstadt, Germany), tetrahydrofuran (THF, 99.5 % stabilized with ~ 300 ppm of BHT, Panreac, Darmstadt, Germany) and ethanol (96 %, Sigma-Aldrich) were used as received. The water used for the OIHs synthesis was high purity deionized water with high resistivity (higher than 18 MΩ cm) obtained from a Millipore water purification system (Milli-Q®, Merck KGaA, Darmstadt, Germany). A simulated concrete pore solution (SCPS) was prepared using deionized water at room temperature. The SCPS was obtained by addition of 0.2 M of KOH (86 %, Absolve) to a $Ca(OH)_2$ (≥95 %, Merck) saturated aqueous solution according to the literature [43] HPLC analysis was performed using required acetonitrile (99.7 %, LAB-SCAN) and glacial acetic acid (99 %).

2.2. Synthesis of organic–inorganic hybrid (OIH) films

Two different samples were prepared: A170 and A170@CTAB@phph (doped with phph). In these designations, the letter "A" is used to identify the type of bond established between the amine end group of the Jeffamine® and the epoxy group of the GPTMS (*i.e.*, amino-alcohol bond: $—[CH(OH)—CH_2—NH]_n—$) that leads to the formation of OIH precursors that are named as conventional amino-alcohol silicates. Furthermore, the numbering identifies the Jeffamine® used in the synthesis (Jeffamine® THF-170).

A170 doped with phph was synthesized. The doped material was prepared by mixing polyetheramine Jeffamine® THF-170 (previously dissolved in THF) and 3-glycidoxipropyltrimethoxysilane (GPTMS) in a glass container. A molar ratio of 2 GPTMS: 1 Jeffamine® was used. The sol was stirred for 20 mins and 200 μL of a 0.1 M CTAB aqueous solution was added. After 10 mins, 400 μL of a 0.1 M phph solution in ethanol was added. The homogeneous sol was cast into a Teflon mould and covered with Parafilm during the gelation process. The OIHs were placed in an oven (UNB 200, Memmert, Buechenbach, Germany) and kept at 40 °C for 15 days to ensure the curing of the films and remaining solvent evaporation. Fig. 1 shows the synthesis steps for the preparation of the A170@CTAB@phph film and its photograph.
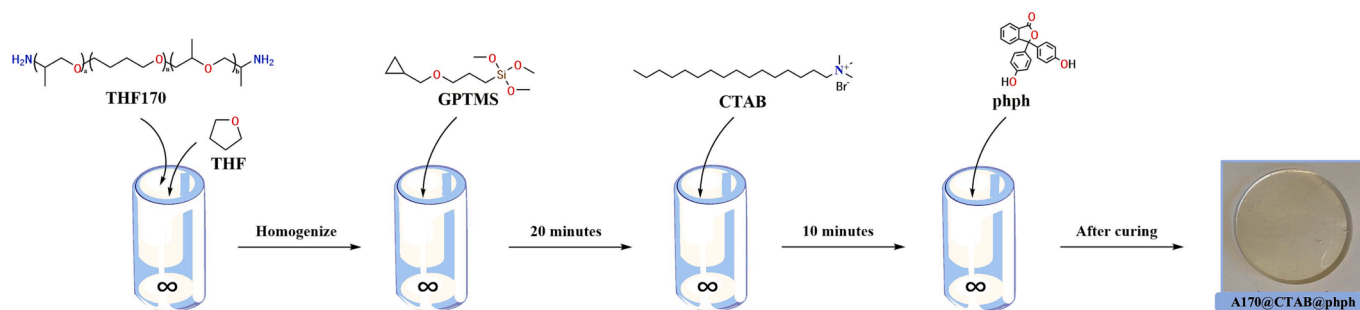
Fig. 1. Synthesis steps of the doped OIH A170.

The pure A170 OIH matrix was synthesized using a procedure similar to the one described elsewhere [36]. However, in the case of pure matrix no CTAB was added and the same quantity of ethanol, without any phph, was used for comparison purposes.

2.3. Characterization of OIH films

2.3.1. Attenuated total reflectance – Fourier transform infrared spectroscopy

FTIR spectra for the OIH films were recorded in absorbance mode on a Perkin Elmer Spectrum Two™ spectrometer, by averaging 64 scans at a maximum resolution of 4 cm^{-1}. Spectra were obtained in 4000–500 cm^{-1} range.

2.3.2. Electrochemical impedance spectroscopy

EIS measurements were carried out at room temperature in a Faraday cage, using a potentiostat/galvanostat/ZRA (Reference 600+, Gamry Instruments, Warminster, PA, USA). EIS measurements were used to characterize the resistance, electrical conductivity, and electric permittivity of the OIHs, as well as their capacitance. EIS measurements were conducted by cutting the OIHs in a disc format, which was placed between two parallel Au electrodes (10 mm diameter and 250 µm thickness) using a support cell, as reported in previous studies [44]. The measurements were accomplished by applying a 10 mV (peak-to-peak, sinusoidal) electrical potential within a frequency range from 1×10^6 Hz to 0.01 Hz at open circuit potential. The frequency response data of the studied electrochemical cells were displayed in a Nyquist plot, using Gamry ESA410 Data Acquisition software which was also used for data fitting purposes.

2.3.3. UV/Vis spectroscopy

UV/Vis spectra of the OIHs were recorded in transmittance and absorbance mode on a Shimadzu UV-2501 PC spectrophotometer. Spectra were obtained in the range of 200–700 nm.

2.3.4. Fluorescence spectroscopy

Fluorescence spectra of the OIHs were recorded on a Fluoromax – 4 Spectrofluorometer (Horiba Jovin Yvon). Spectra were obtained in the range of 300–700 nm, with different excitation wavelengths and acquired at front-face geometry at room temperature.

2.3.5. Thermogravimetric analysis

TGA was carried out on a TA Instruments SDT Q600 system. Samples were subjected to a temperature ramp of 15 °C min^{-1} from room temperature to 750 °C, at a constant 100 mL min^{-1} nitrogen flux. For each analysis, 20 – 30 mg of each OIH was placed into an alumina pan.

2.3.6. Phenolphthalein release studies

For the phph release study, a 1 cm diameter disc cut from the original A170@CTAB@phph film was used. The sample was placed successively in 27 plastic flasks containing 12 mL of SCPS. The time that the sample remained in each of the flasks increased throughout the study. The analysis of each means of release was performed, as soon as possible, after the removal of the sample from each flask and involved, firstly, their acidification with glacial acetic acid to a pH of approximately 2.5 and, secondly, their injection into the HPLC.

2.3.7. HPLC-UV analysis

High-performance liquid chromatography (HPLC) system consists of an isocratic pump (Jasco PU-2080 Plus) and a UV–vis detector (Shimadzu SPD-6A). The product partition was carried out using GraceSmart RP-18 analytical column (250 × 4.6 mm, 5 µm) and ACN:H$_2$O (1:3) mixture as mobile phase. Phph was quantified at 230 nm.

3. Results and discussion

3.1. Organic-inorganic hybrids (OIHs) as pH sensors

In previous work carried out by some members of our research group, several OIHs were synthesized and characterized for application in highly alkaline environment (cement paste) [36]. From the previously reported matrices, only A170 proved to have the necessary properties to resist the strongly alkaline environment such as the one found in concrete, since it was the only one that did not suffer relevant degradation after 28 days of contact with a cement paste. Furthermore, due to its optical and electrical properties, and chemical stability, it seems to be a promising OIH to be applied in optical sensors for application in the civil engineering field [36]. For that reason, in this work, a A170 matrix has been doped with phph and CTAB to develop a pH-responsive OIH material. As a proof of concept of the synthesized OIHs, a drop of the prepared SCPS was added on top of OIH samples doped and undoped with phph. Fig. 2 shows that A170@CTAB@phph colour changed in contact with the alkaline environment, *i.e.*, SCPS (pH > 12.5), just as envisioned.

3.2. Attenuated total reflectance – Fourier transform infrared spectroscopy analysis

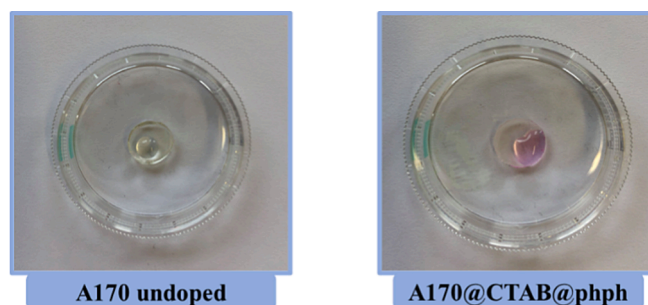FTIR-ATR analysis was performed for the OIHs materials

Fig. 2. Synthetized OIHs with the addition of one drop of the SCPS (pH > 12.5).

synthesized. The spectra obtained for these samples are shown in Fig. 3. In addition, spectra of the precursors have also been plotted and can be found in supplementary material (Figs. S1 and S2).

Fig. S1 show the peaks at 1492 and 1371 cm^{-1} which correspond to the Jeffamine® THF170 carbon chain. In the A170 spectrum, these same peaks are observed with small differences which indicates that the carbon chain of Jeffamine® THF170 has not changed [45]. On the other hand, the epoxy ring of GPTMS (3049 cm^{-1} – Fig. S2) disappeared, which indicates that the reaction between the two precursors took place. Furthermore, the peak at 1190 cm^{-1} (characteristic of Si-OCH$_3$ band) [46], related to the inorganic precursor, observed in Fig. S2, also disappeared, which proves that the hydrolysis of the silane was successfully achieved [47,48]. The peak at 1101 cm^{-1} corresponds to the Si-O-Si bonds characteristic of the cross-linked OIH and the signal at 1242 cm^{-1} can be attributed to the symmetric stretching of the C-Si bond. The bands at 2915 and 2936 cm^{-1} are caused by the asymmetric bending of the C—CH$_2$ bond and the peak at 2854 cm^{-1} is related to the symmetric bending of this same bond [45,48]. An important peak occurs at 1647 cm^{-1} since it corresponds to the C—NH—C bond, which is a part of the amino alcohol bond established between the two precursors [47,48], confirming the success of the synthetic procedure. A broad band is observed at 3433 cm^{-1}, characteristic of the hydroxyl group, which can be caused by the presence of this group either in the polyetheramine chain or by the water molecules that may still be trapped in the polymeric OIH matrix [45].

In the A170@phph infrared spectrum (Fig. S3), and additionally to the signals reported above, a small peak at 1770 cm^{-1} is observed, which is characteristic of the carbonyl group present in the structure of phenolphthalein, this confirms the integration of the dopant in the OIH matrix [49]. In the A170@CTAB@phph infrared spectrum, Fig. 3 shows all the peaks mentioned so far, plus the peak at 3016 cm^{-1}, which can be attributed to the vibration of the C—H bond bending of the —CH$_2$ and —CH$_3$ groups of CTAB [39]. Furthermore, in this spectrum, there were two inversions in the intensity of the bands: one in the band between 1420 and 1503 cm^{-1} (present in all three OIH spectra), and another

between 2890 and 2996 cm^{-1} (whose assignments of the peaks at 2916 and 2934 cm^{-1} have been discussed earlier). This reversal in the intensity of these bands is related with the incorporation of the dopants and the possible formation of bonds between them and the matrix. However, it was not possible to confirm the type of bonds or disruption that occurred upon dopant incorporation.

3.3. Electrochemical impedance spectroscopy analysis

EIS is a technique often used in the characterization of materials, such as OIHs sol–gel material, for the assessment of their dielectric properties [50,51]. The experimental and fitting results are shown in the Nyquist plots in Fig. 4. The equivalent electrical circuits (EEC) used for each sample were also introduced as inset in each Nyquist plot.

EIS was used in this work to characterize the dielectric properties (e. g., conductivity, capacitance, and permittivity). Furthermore, the OIHs resistance values can assess their potential to be used in concrete structures, since it was previously reported that OIHs with resistances values above 10^7 Ω cm^2 are considered suitable for application in high alkalinity environments, such as concrete [52,53].

Nyquist plots are presented since this type of plot shows the capacitive response over a wide range of frequencies. Data obtained in the high-frequency zone of this type of plot can be used to assess the abovementioned dielectric properties of the material. Fig. 4 shows that the two OIHs describe a semi-circle that intersects the x axis. The amplitude of the semi-circle changes with the sample's composition, i.e., with the presence of phph. It can also be observed that, at lower frequencies, a different electrochemical process is present. However, no further conclusions can be drawn.

The analysis of EIS data was performed based on the represented EEC and the corresponding fitting parameters are shown in Table 1. The resistance of the films (R$_{sample}$), constant phase elements (CPE was used instead of pure capacitance to improve the data fitting since the data do not show ideal behaviour), parameter independent of frequency (α) and goodness of fit (χ^2) are shown.
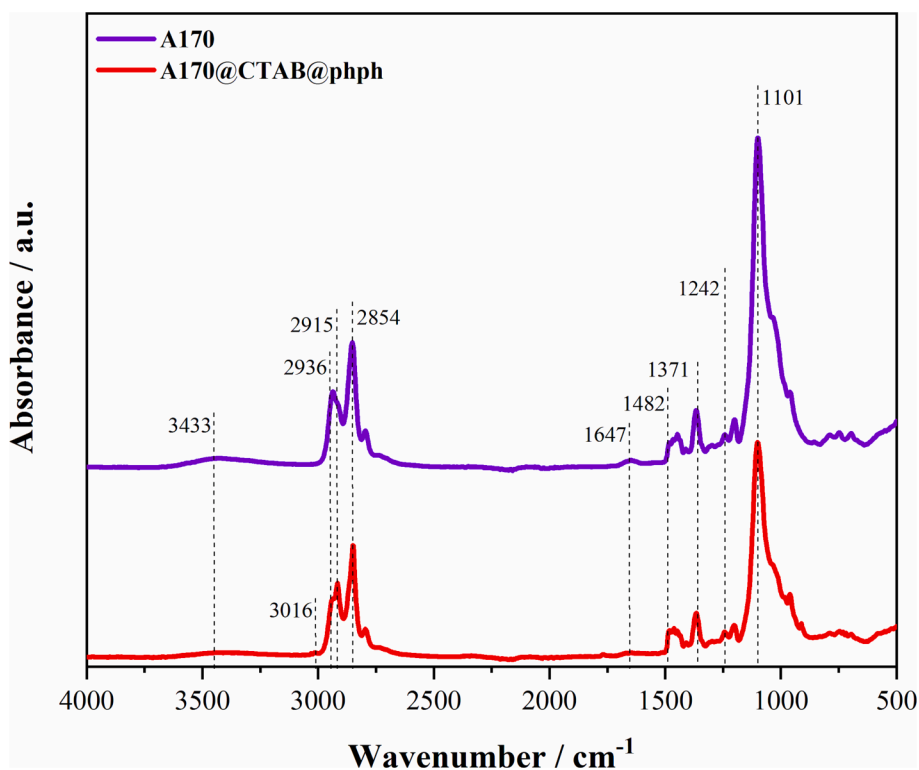
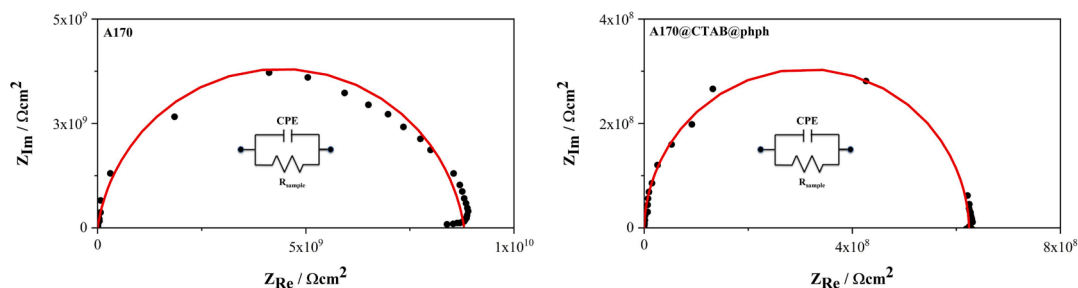

Fig. 3. FTIR spectra of synthesized films.

Fig. 4. Nyquist plots obtained for the OIHs.

Table 1
Values of elements of the proposed EEC obtained from EIS data fitting of the OIHs.

OIHs	R_{sample}/Ω cm^2	CPE (Q)/S^α Ω^{-1} cm^{-2}		χ^2
A170	8.80×10^9	6.91×10^{-12}	0.91	3.03×10^{-3}
A170@CTAB@phph	6.24×10^8	6.57×10^{-12}	0.98	2.64×10^{-3}

The resistance of the A170@CTAB@phph is above 10^7 Ω meaning that the OIH obtained is suitable for concrete sensing purposes [53]. R_{Sample}, CPE, and α were used to obtain the effective capacitance (C_{eff}) by using the Brug *et al.* relationship [54]. Resistance (R), capacitance (C), conductivity (σ), and relative permittivity (ε_r) values were obtained using the Eqs. (1)–(4), respectively. The values are shown in Table 2 and were normalized to the cell geometry dimensions, with A_{Au} standing for the gold electrodes' area, d_{Sample} for the thickness of the sample, and ε_0 for vacuum permittivity.

$$R = R_{sample} \times A_{Au\ dis} \tag{1}$$

$$C = C_{eff}/A_{Au\ disc} \tag{2}$$

$$\sigma = \left(d_{sample}/A_{Au\ disc}\right)/R_{sample} \tag{3}$$

$$\varepsilon_r = \left(\left(C_{eff} \times d_{sample}\right)/\varepsilon_0\right) \times A_{Au\ disc} \tag{4}$$

The logarithm of resistance obtained for the synthesized OIH membranes is between 10.19 and 7.06 Ω cm^2, with the matrix showing a higher value when compared to A170@CTAB@phph (*vide* Table 2). These results are in agreement with previous studies of doped A170 materials with organic-based molecules, showing higher resistance [37]. The C value obtained is between 5.53 and 7.61 pF cm^{-2}, where A170 and A170@CTAB@phph showed the lowest and highest value, respectively. As for the dielectric constant, it ranges between 10.33 and 11.77, in which the lowest value corresponds to the A170@CTAB@phph and the highest to the A170. It can be observed that the resistances are higher than 10^7 Ω cm^2 which allow to show that the materials show dielectric properties that are suitable for alkaline environments [53].

3.4. UV/Vis spectroscopy analysis

UV/Vis spectroscopy allows to assess the transparency and

Table 2
Electrical properties of the OIHs.

OIHs	log R/Ω cm^2	C/pF cm^{-2}	$-log \sigma$/S cm^{-1}	ε_r
A170	10.19 ± 0.28	5.53 ± 0.89	10.91 ± 0.28	11.77 ± 1.89
A170@CTAB@phph	7.06 ± 1.53	7.61 ± 0.16	9.61 ± 0.02	10.3 ± 0.21

absorbance of OIH films. Fig. 5 shows the optical transmittance and absorbance spectra as a function of wavelength obtained for the obtained OIHs, respectively.

Observing the results obtained in spectra it is noteworthy that, at a wavelength of 400 nm, A170 shows a high transmittance (above 70 %), unlike A170@CTAB@phph which shows lower transmittance values (<40 %). Thus, A170@CTAB@phph shows the lowest transparency. Queiroz *et al.* [55] reported that the transmittance changes depend on the particle size which has the ability to transmit light accordingly. The presence of pores caused by the CTAB surfactant could be the reason why the light is scattered which consequently causes the decreasing transparency of the material. The spectrum of the A170@phph material is shown in supplementary material (Fig. S5).

3.5. Fluorescence spectroscopy analysis

The doped effect was further assessed by fluorescence spectroscopy on the samples in solid state. Fig. 7 shows the fluorescence emission spectrums of synthesized OIH films.

Through the analysis of the Fig. 6 (left side), it is possible to observe that A170 shows intrinsic fluorescence [36]. In these OIHs, the intrinsic fluorescence emission is associated with photo-induced proton transfer between NH^+/NH^- and with electron-hole recombination occurring in the GPTMS nanoclusters and this is according to the literature [36]. It is also observed that with the increase of the excitation wavelength, the emission peak shifts to longer wavelengths The emission wavelength dependency with the excitation energy is related to the size of the silica clusters and to unorganized processes that are generally linked to transitions that occur between localized states in non-crystalline structures [56,57]. Analysing Fig. 6 regarding A170@CTAB@phph sample (right side) shows the same shifting behaviour as the undoped matrix.

Another OIH was synthesized using the same procedure of A170@CTAB@phph, an OIH doped with only phph (A170@phph) which can be found in the supplementary material section (Fig. S6). Considering all three spectra, the position of the emission peak of the OIHs, for the excitation wavelengths used, does not change significantly. However, it can be detected that the characterized films exhibit their maximum emission peak at different excitation wavelengths. For A170, it occurs at a wavelength of 360 nm, for A170@phph it occurs at a wavelength of 350 nm, and for A170@CTAB@phph it occurs at a wavelength of 370 nm. Thus, a hypsochromic and bathochromic deviation of the maximum emission peak, relative to the matrix, is observed for the A170@phph and A170@CTAB@phph OIHs, respectively. Regarding the fluorescence intensity, it is noteworthy that there is a hyperchromic shift in the doped OIH compared to the matrix ($\lambda^{max} = 435$ nm and $\lambda^{max} = 1.09x10^7$ nm). In the case of A170@phph, this deviation ($\lambda^{max} = 424$ nm and $\lambda^{max} = 1.18x10^7$) is not substantial, on the other hand, in the case of A170@CTAB@phph ($\lambda^{max} = 436$ nm and $\lambda^{max} = 1.58x10^7$ nm), it is considerable and, therefore, it appears that a synergistic effect of the phph and CTAB in the intrinsic fluorescence of the matrix may be the explanation for such behaviour. Nevertheless, the results show that no significant changes are found in the intrinsic fluorescence of the matrices and no interference is expected to occur in the
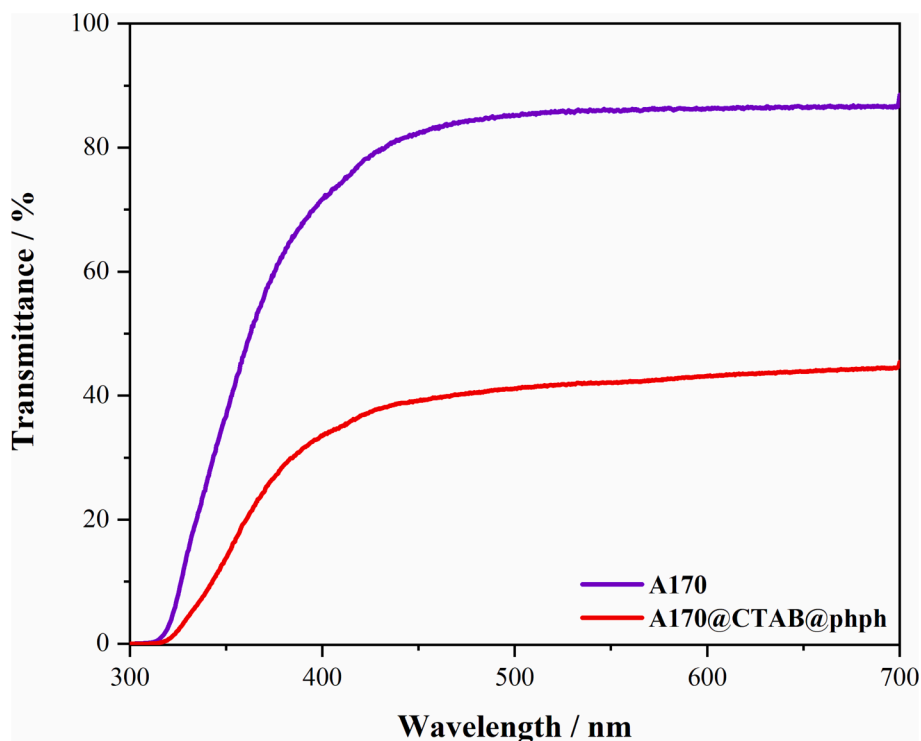
Fig. 5. UV/Vis transmittance spectra of synthesized films.
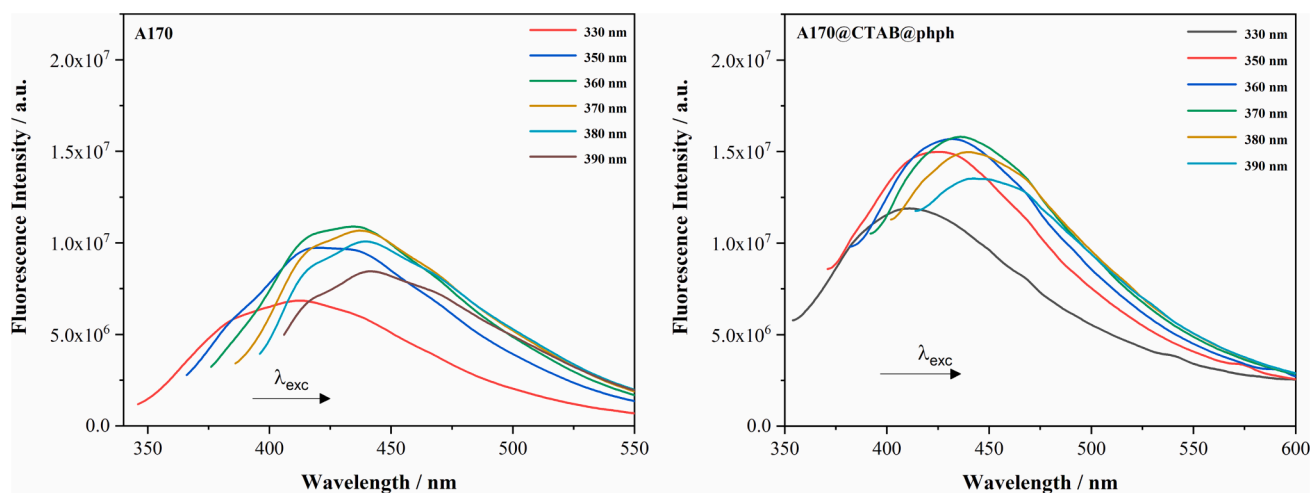

Fig. 6. Fluorescence emission spectra of synthesized films. Left-side and right-side regards to A170 and A170@CTAB@phph OIH matrixes, respectively.

colourimetric response.

3.6. Thermogravimetric analysis

Fig. 7 shows TGA and the corresponding DTG for A170 and A170@CTAB@phph. Observing the thermograms presented, it can be seen that the OIH exhibit only one degradation process, between 375 and 450 °C, which is in agreement with the results previously reported [36]. Results on the literature show that, for this type of OIHs, the highest degradation processes occur between 350 and 500 °C, due to depolymerization of the Jeffamine moiety and residual condensation of Si–OH group [47,58–60].

Table 3 shows the 5 % weight loss temperature (T_5), the temperature of the maximum rate of weight loss (T_{max}) and the char yield, for the OIHs. T_5 values are slightly lower for the doped OIHs, which may be due

to the evaporation of residual solvents entrapped within the matrix, added with the doping agents. T_{max} is higher for doped films when compared to undoped ones, however, the difference is not significant to draw further conclusions. Char yield values show a higher percentage of residual weight at 750 °C for A170, suggesting lower crosslinking density for the doped films, which is according to data previously reported [37]. In general, the results show that no major changes are seen in the thermal profile of the OIHs. For the proposed application, the films may be applied on fresh concrete, since concrete curing processes do not reach temperatures above 70 °C [61].

3.7. Stability studies of OIH matrix doped with phph when immersed in SCPS

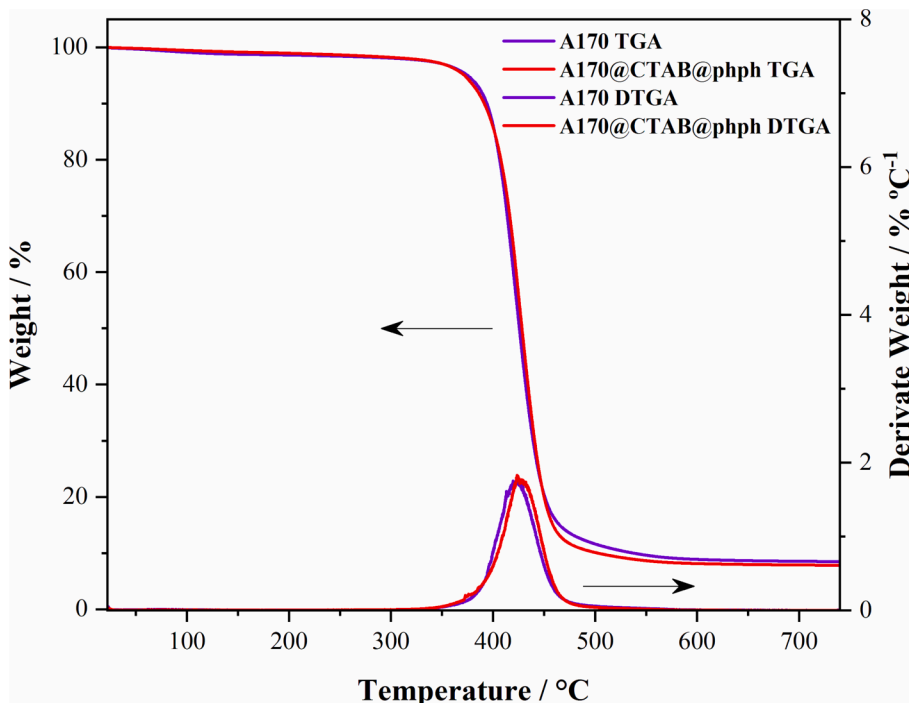The presence of water inside the concrete pores can be a drawback

Fig. 7. TGA and DTGA traces for the OIH films.

Table 3
5% weight loss temperature (T_5), the temperature of the maximum rate of weight loss (T_{max}) and Char Yield for the OIHs (data obtained from the TGA and DTGA traces).

OIH films	T_5 (°C)	T_{max} (°C)	Char Yield (%)
A170	375	423	8.4
A170@CTAB@phph	372	430	7.8

for the RCS but also to develop a stable pH sensor. Despite the low solubility of phph in water (3.36 mg L^{-1} at 20 °C) [62], the herein proposed OIH could lose phph (the pH sensing molecule) by releasing it in an aqueous media. This is particularly critical in certain environments such as bridges and dams. Therefore, understanding of phph stability within the OIH network is crucial to assess the durability of the pH sensor. To assess this shortcoming, and due to the difficulty to determine the concentration of phph directly released from the OIH to the concrete, some extreme experimental conditions (regarding the expected real conditions) were conducted by immersing the A170@CTAB@phph in a SCPS, while monitoring the release of phph by HPLC.

When the A170@CTAB@phph sample was immersed in the SCPS, the solution colour changed from colourless to pink, showing the release of phph from the OIH into the aqueous media (*vide*, Fig. 2). Fig. 8A) shows the kinetics release of phph in the SCPS.

From Fig. 8A) it can be observed that after 430 h (*ca.* 18 days) the cumulative amount of phph released is equal to 93.3 mg mL^{-1}, which corresponds to a cumulative release of 96 % of the encapsulated phph. However, to have a deep assessment of the release kinetics and release mechanism, several models have been used.
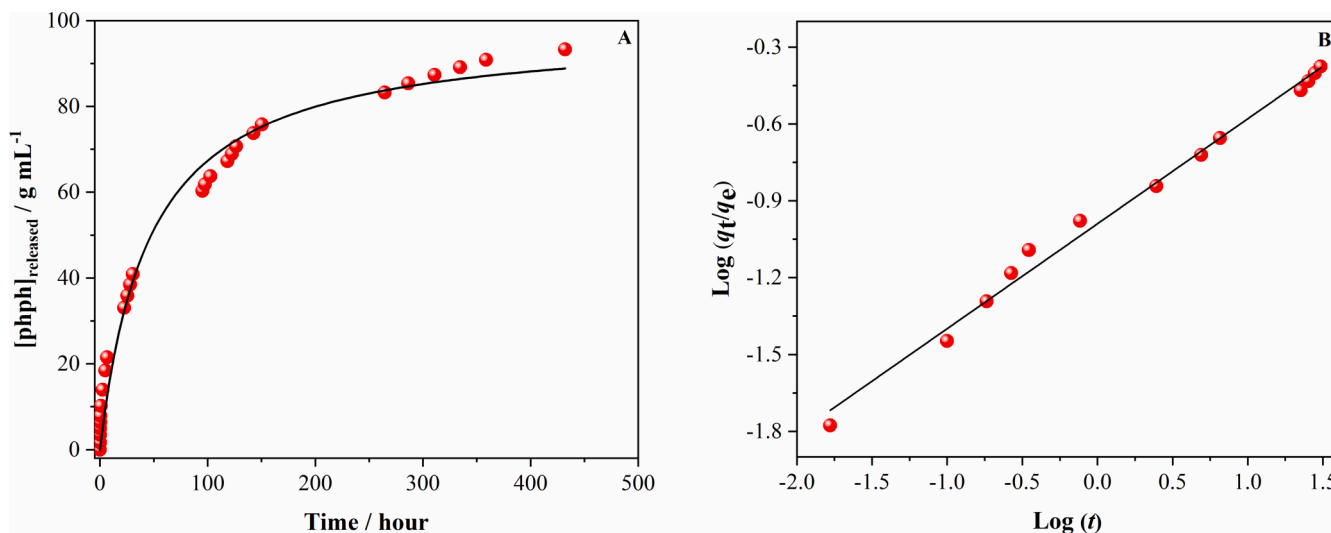

Fig. 8. A) Cumulative release of phph from OIH matrix as a function of time and B) application of the linearized form of the power law equation (Eq. (5)) to the experimental release data for short-range times ($q_t/q_e < 0.6$).

Initially, the pseudo-first and pseudo-second order (PSO) equations have been fitted to the experimental data. Once the finest fit has been obtained with the latter, only that one is considered, described, and discussed. Thus, the PSO equation can be defined as [63,64]:

$$\frac{\mathrm{d}q_t}{\mathrm{d}t} = k_2(q_e - q_t)^2 \tag{5}$$

where q_t and q_e (both in g mL^{-1}) are the amounts of phph released at time t and at equilibrium, respectively, and k_2 is the pseudo-second (mL g^{-1}h^{-1}) order release rate constant. By integrating Eq. (5), assuming the following initial and boundary conditions $t = 0$ and $q_t = 0$, and for $t > 0$, $q_t = f(t)$ (*i.e.*, infinite volume assumption), the following equation is obtained (Eq. (6)):

$$q_t = \frac{q_e^2 k_2 t}{1 + q_e k_2 t} \tag{6}$$

The fitting of Eq. (6) to experimental data (*vide* solid line in Fig. 8A) leads to a $q_e = 98 \, (\pm 3)$ g mL^{-1} and a $k_2 = 2.2 \, (\pm 0.3) \times 10^{-4}$ mL g^{-1}h^{-1}, with a determination coefficient equal to 0.9791, which corresponds to very slow-release kinetics. Additionally, the computed q_e value agrees with the experimental one (97.2 g mL^{-1}).

A different approach is based on the analysis of the release kinetics for short-range times (*i.e.*, $q_t/q_e < 0.6$). For those conditions, the power law equation [65] and the mean dissolution time (*MDT*) can be evaluated by using Eqs. (7) and (8), respectively.

$$q_t/q_e = kt^n \tag{7}$$

$$MDT = \left(\frac{n}{n+1}\right) k^{-n^{-1}} \tag{8}$$

where and k and n are fitting parameters, giving the latter useful information on the release mechanism; from the fitting procedure (*vide* Fig. 8B)) a n value equal to 0.41 (± 0.1) is obtained, indicating that the release of phph for short-range times is mainly driven by its concentration gradient (*i.e.*, the release follows a Fickian behaviour) [66]. Considering the fitting parameters n and k, the *MDT* can be calculated and, for this system, is equal to 75.4 (± 0.02) hours. This parameter is a measure of the phph release-retarding efficiency of the encapsulation which can be considered quite effective.

4. Conclusion

OIH with pH sensing ability were successfully synthesized by using GPTMS and Jeffamine® THF-170 as precursors with CTAB as surfactant and phph as a doping material.

ATR-FTIR spectroscopy confirmed that the reaction between the matrix precursors is the amino-alcohol type and proved that the incorporation of these phph does not affect the chemical structure of the OIH matrix. EIS showed that the resistance values are higher than $10^7 \, \Omega \, \text{cm}^2$, which indicates that the OIHs show dielectric properties suitable for alkaline environments such as concrete and the presence of phph do not interfere significantly with the OIH dielectric properties. Through the results obtained by UV/Vis spectroscopy, it was shown that the matrix displays high transmittance values for wavelengths longer than 400 nm. However, the transmittance of the synthesized A170@CTAB@phph showed the lowest transparency. The analysis of the OIHs by fluorescence spectroscopy indicates that the OIH matrix has intrinsic fluorescence and that doping the matrix only caused small deviations in the wavelength of the peak of maximum emission. TGA data proved that the produced OIHs were stable enough to be used in fresh concrete since their thermal degradation only occurs for values above the ones that are usually during the curing process of concrete. Stability tests of phph in the OIH matrix proved that measure of the phph release-retarding efficiency of the encapsulation can be considered quite effective. In the end, it is possible to conclude that these OIH membranes showed relevant

potential to be used as sensing materials to assess the pH of concrete.

CRediT authorship contribution statement

Bárbara Ferreira: Investigation, Writing – original draft, Data curation, Formal analysis. **Sara Sousa:** Investigation, Writing – original draft, Formal analysis. **Rui P.C.L. Sousa:** Writing – review & editing. **Susana P.G. Costa:** Visualization. **M. Manuela M. Raposo:** Visualization. **Pier Parpot:** Visualization. **Artur J.M. Valente:** Visualization. **Rui F.P. Pereira:** Conceptualization, Methodology, Formal analysis, Writing – review & editing, Project administration, Supervision. **Rita B. Figueira:** Conceptualization, Methodology, Formal analysis, Writing – original draft, Project administration, Supervision, Funding acquisition.

Declaration of Competing Interest

The authors declare that they have no known competing financial interests or personal relationships that could have appeared to influence the work reported in this paper.

Data availability

No data was used for the research described in the article.

Appendix A. Supplementary data

Supplementary data to this article can be found online at https://doi.org/10.1016/j.conbuildmat.2022.129493.

References

[1] R.B. Figueira, Electrochemical sensors for monitoring the corrosion conditions of reinforced concrete structures: a review, Appl. Sci. 7 (2017), https://doi.org/10.3390/app7111157.

[2] H. Böhni, Corrosion in reinforced concrete structures, Elsevier, 2005.

[3] R.B.P.L. Bertolini, B. Elsener, P. Pedeferri, Corrosion of Steel in Concrete, in: R. W. Revie (Ed.), Prevention, Diagnosis, Repair, Second Edi, Wiley, 2005, p. 409, https://doi.org/10.1002/3527603379.

[4] M.A. Baccay, N. Otsuki, T. Nishida, S. Maruyama, Influence of cement type and temperature on the rate of corrosion of steel in concrete exposed to carbonation, Corrosion 62 (2006) 811–821, https://doi.org/10.5006/1.3278306.

[5] F. Duprat, N.T. Vu, A. Sellier, Accelerated carbonation tests for the probabilistic prediction of the durability of concrete structures, Constr. Build. Mater. 66 (2014) 597–605, https://doi.org/10.1016/j.conbuildmat.2014.05.103.

[6] A. Belda Revert, K. De Weerdt, K. Hornbostel, M.R. Geiker, Carbonation-induced corrosion: investigation of the corrosion onset, Constr. Build. Mater. 162 (2018) 847–856, https://doi.org/10.1016/j.conbuildmat.2017.12.066.

[7] C. Andrade, Evaluation of the degree of carbonation of concretes in three environments, Constr. Build. Mater. 230 (2020), 116804, https://doi.org/10.1016/j.conbuildmat.2019.116804.

[8] L. Bertolini, Steel corrosion and service life of reinforced concrete structures, Struct. Infrastruct. Eng. 4 (2008) 123–137, https://doi.org/10.1080/15732470601155490.

[9] S. Park, S. Ahmad, C.B. Yun, Y. Roh, Multiple crack detection of concrete structures using impedance-based structural health monitoring techniques, Exp. Mech. 46 (2006) 609–618, https://doi.org/10.1007/s11340-006-8734-0.

[10] M. Usman Rashid, Experimental investigation on durability characteristics of steel and polypropylene fiber reinforced concrete exposed to natural weathering action, Constr. Build. Mater. 250 (2020), 118910, https://doi.org/10.1016/j.conbuildmat.2020.118910.

[11] I.A. Korotchenko, E.N. Ivanov, S.S. Manovitsky, V.A. Borisova, K.V. Semenov, Y.G. Barabanshchikov, Deformation of concrete creep in the thermal stress state calculation of massive concrete and reinforced concrete structures, Magazine of, Civ. Eng. 69 (2017) 56–63, https://doi.org/10.18720/MCE.69.5.

[12] B.S. Jang, B.H. Oh, Effects of non-uniform corrosion on the cracking and service life of reinforced concrete structures, Cem. Concr. Res. 40 (2010) 1441–1450, https://doi.org/10.1016/j.cemconres.2010.03.018.

[13] T.H. Nguyen, T. Venugopala, S. Chen, T. Sun, K.T.V. Grattan, S.E. Taylor, P.A.M. Basheer, A.E. Long, Fluorescence based fibre optic pH sensor for the pH 10–13 range suitable for corrosion monitoring in concrete structures, Sens. Actuators B, Chem. 191 (2014) 498–507, https://doi.org/10.1016/j.snb.2013.09.072.

[14] J. Zhang, H. Dongwei, S. Wei, Experimental study on the relationship between shrinkage and interior humidity of concrete at early age, Mag. Concr. Res. 62 (2010) 191–199, https://doi.org/10.1680/macr.2010.62.3.191.

[15] B.H. Oh, S.Y. Jang, Effects of material and environmental parameters on chloride penetration profiles in concrete structures, Cem. Concr. Res. 37 (2007) 47–53, https://doi.org/10.1016/j.cemconres.2006.09.005.

[16] D. Xu, S. Banerjee, Y. Wang, S. Huang, X. Cheng, Temperature and loading effects of embedded smart piezoelectric sensor for health monitoring of concrete structures, Constr. Build. Mater. 76 (2015) 187–193, https://doi.org/10.1016/j.conbuildmat.2014.11.067.

[17] S. Taheri, A review on five key sensors for monitoring of concrete structures, Constr. Build. Mater. 204 (2019) 492–509, https://doi.org/10.1016/j.conbuildmat.2019.01.172.

[18] J.-A. Jeong, C.-K. Jin, Y.-H. Kim, W.-S. Chung, Electrochemical Performance Evaluation of Corrosion Monitoring Sensor for Reinforced Concrete Structures, J. Adv. Concr. Technol. 11 (2013) 1–6, https://doi.org/10.3151/jact.11.1.

[19] E.V. Pereira, R.B. Figueira, M.M. Salta, I.T.E. Fonseca, Embedded sensors for corrosion monitoring of existing reinforced concrete structures, Mater. Sci. Forum 587–588 (2008) 677–681, https://doi.org/10.4028/www.scientific.net/MSF.587-588.677.

[20] E.V. Pereira, R.B. Figueira, M.M.L. Salta, I.T.E. da Fonseca, A galvanic sensor for monitoring the corrosion condition of the concrete reinforcing steel: relationship between the galvanic and the corrosion currents, Sens. (Basel). 9 (2009) 8391–8398, https://doi.org/10.3390/s91108391.

[21] C.I. Merzbacher, A.D. Kersey, E.J. Friebele, Fiber optic sensors in concrete structures: a review, in: K.T.V. Grattan, B.T. Meggitt (Eds.), Optical Fiber Sensor Technology: Applications and Systems, Springer, US, Boston, MA, 1999, pp. 1–24, https://doi.org/10.1007/978-1-4757-6077-4_1.

[22] K. Kesavan, K. Ravisankar, S. Parivallal, P. Sreeshylam, S. Sridhar, Experimental studies on fiber optic sensors embedded in concrete, Measurement 43 (2010) 157–163, https://doi.org/10.1016/j.measurement.2009.08.010.

[23] X. Zhao, P. Gong, G. Qiao, J. Lu, X. Lv, J. Ou, Brillouin corrosion expansion sensors for steel reinforced concrete structures using a fiber optic coil winding method, Sensors 11 (2011) 10798–10819, https://doi.org/10.3390/s111110798.

[24] D. Luo, Y. Yue, P. Li, J. Ma, L. ling Zhang, Z. Ibrahim, Z. Ismail, Concrete beam crack detection using tapered polymer optical fiber sensors, Measurement 88 (2016) 96–103, https://doi.org/10.1016/j.measurement.2016.03.028.

[25] A. Barrias, J.R. Casas, S. Villalba, Embedded distributed optical fiber sensors in reinforced concrete structures—a case study, Sensors 18 (2018) 980, https://doi.org/10.3390/s18040980.

[26] W. Grahn, P. Makedonski, J. Wichern, W. Kowalsky, S. Wiese, Fiber optic sensors for an in-situ monitoring of moisture and pH value in reinforced concrete, Imaging Spectrom. VII. 4480 (2002) 395, https://doi.org/10.1117/12.453362.

[27] M.P. Basheer, K.T.V. Grattan, T. Sun, A.E. Long, D. McPolin, W. Xie, Fiber optic chemical sensor systems for monitoring pH changes in concrete Advanced Environmental, Chem. Biol. Sens. Technol. II (5586) (2004) 144, https://doi.org/10.1117/12.601198.

[28] W. Xie, T. Sun, K.T.V. Grattan, D. McPolin, P.A.M. Basheer, A.E. Long, Fibre optic chemical sensor systems for internal concrete condition monitoring, in: Second European Workshop on Optical Fibre Sensors, International Society for Optics and Photonics, 2004, pp. 334–337, https://doi.org/10.1117/12.566705.

[29] D.O. Mcpolin, P.A.M. Basheer, K. Grattan, A. Long, T. Sun, W. Xie, Preliminary development and evaluation of fibre optic chemical sensors, J. Mater. Civ. Eng. 23 (2011) 1200–1210, https://doi.org/10.1061/(ASCE)MT.1943-5533.0000290.

[30] S. Islam, N. Bidin, S. Riaz, G. Krishnan, S. Daud, S. Naseem, F.M. Marsin, Sol-gel based optically active phenolphthalein encapsulated nanomatrices for sensing application, J. Sol-Gel Sci. Technol. 79 (2016) 616–627, https://doi.org/10.1007/s10971-016-4041-0.

[31] S. Islam, N. Bidin, S. Riaz, G. Krishnan, S. Naseem, Sol-gel based fiber optic pH nanosensor: structural and sensing properties, Sens. Actuators, A 238 (2016) 8–18, https://doi.org/10.1016/j.sna.2015.12.003.

[32] S. Islam, N. Bidin, S. Riaz, S. Naseem, Self-assembled hierarchical phenolphthalein encapsulated silica nanoparticles: structural, optical and sensing response, Sens. Actuators, A 266 (2017) 111–121, https://doi.org/10.1016/j.sna.2017.09.020.

[33] C. Grengg, B. Müller, C. Staudinger, F. Mittermayr, J. Breininger, B. Ungerböck, S.M. Borisov, T. Mayr, M. Dietzel, High-resolution optical pH imaging of concrete exposed to chemically corrosive environments, Cem. Concr. Res. 116 (2019) 231–237, https://doi.org/10.1016/j.cemconres.2018.10.027.

[34] B. Inserra, K. Hayashi, A. Marchisio, J.-M. Tulliani, Sol–gel-entrapped pH indicator for monitoring pH variations in cementitious materials, J. Appl. Biomater. Funct.

[35] J. Bartelmess, D. Zimmek, M. Bartholmai, C. Strangfeld, M. Schäferling, Fibre optic ratiometric fluorescence pH sensor for monitoring corrosion in concrete, Analyst. 145 (2020) 2111–2117, https://doi.org/10.1039/c9an02348h.

[36] B.R. Gomes, R.B. Figueira, S.P.G. Costa, M.M.M. Raposo, C.J.R. Silva, Synthesis Optical and Electrical Characterization of Amino-alcohol Based Sol-gel Hybrid Materials, Polymers 12 (2020) 2671, https://doi.org/10.3390/polym12112671.

[37] R.P.C.L. Sousa, R.B. Figueira, B.R. Gomes, S.P.G. Costa, M. Azenha, R.F.P. Pereira, M. Manuela Raposo, Organic–inorganic sol–gel materials doped with a fluorescent triarylimidazole derivative, RSC Adv. 11 (2021) 24613–24623, https://doi.org/10.1039/D1RA03997K.

[38] C. Rottman, G. Grader, Y. De Hazan, S. Melchior, D. Avnir, Surfactant-induced modification of dopants reactivity in sol–gel matrixes, J. Am. Chem. Soc. 121 (1999) 8533–8543, https://doi.org/10.1021/ja991269p.

[39] S. Islam, R. Rahman, Z. Othaman, S. Riaz, S. Naseem, Synthesis and characterization of hybrid matrix with encapsulated organic sensing dyes for pH sensing application, J. Ind. Eng. Chem. 20 (2014) 4408–4414, https://doi.org/10.1016/j.jiec.2014.02.008.

[40] C.-F. Chang, J.-W. Chen, The experimental investigation of concrete carbonation depth, Cem. Concr. Res. 36 (2006) 1760–1767, https://doi.org/10.1016/j.cemconres.2004.07.025.

[41] Y. Lo, H.M. Lee, Curing e ects on carbonation of concrete using a phenolphthalein indicator and Fourier-transform infrared spectroscopy, Build. Environ. 8 (2002).

[42] H.J. Lee, D.G. Kim, J.H. Lee, M.S. Cho, A study for carbonation degree on concrete using a phenolphthalein indicator and fourier-transform infrared spectroscopy, Int. J. Civ. Environ. Eng. (2012) 7.

[43] C. Andrade, C. Alonso, Corrosion rate monitoring in the laboratory and on-site, Constr. Build. Mater. 10 (1996) 315–328, https://doi.org/10.1016/0950-0618(95)00044-5.

[44] R. Figueira, E. Callone, C. Silva, E. Pereira, S. Dirè, Hybrid coatings enriched with tetraethoxysilane for corrosion mitigation of hot-dip galvanized steel in chloride contaminated simulated concrete pore solutions, Materials 10 (2017) 306, https://doi.org/10.3390/ma10030306.

[45] J. Coates, Encyclopedia of Analytical Chemistry, Am. Cancer Soc. (2006).

[46] P.J. Launer, Infrared Analysis of Organosilicon Compounds, in: Silicon Compounds: Silanes & Silicones, 3rd ed., Gelest Inc., 2013: pp. 175–178.

[47] S.D.F.C. Moreira, C.J.R. Silva, L.A.S.A. Prado, M.F.M. Costa, V.I. Boev, J. Martín-Sánchez, M.J.M. Gomes, Development of new high transparent hybrid organic-inorganic monoliths with surface engraved diffraction pattern, J. Polym. Sci., Part B: Polym. Phys. 50 (2012) 492–499, https://doi.org/10.1002/polb.23028.

[48] B. Arkles, Silicon compounds, silanes, in: Kirk-Othmer Encyclopedia of Chemical Technology, American Cancer Society, 2000, https://doi.org/10.1002/0471238961.1909120101181112.a01.

[49] S. Islam, N. Bidin, S. Riaz, S. Naseem, Sol–gel based phenolphthalein encapsulated heterogeneous silica–titania optochemical pH nanosensor, J. Ind. Eng. Chem. 34 (2016) 258–268, https://doi.org/10.1016/j.jiec.2015.11.022.

[50] J.R. Macdonald, Impedance Spectroscopy Emphasizing Solid Materials and Analysis, John Wiley & Sons Ltd, New York, NY, USA, 1987.

[51] M.E. Orazem, B. Tribollet, Electrochemical Impedance Spectroscopy, John Wiley and Sons, Ltd., New York, NY, USA, 2008.

[52] R.B. Figueira, C.J. Silva, E.V. Pereira, M.M. Salta, Ureasilicate hybrid coatings for corrosion protection of galvanized steel in cementitious media, J. Electrochem. Soc. 160 (2013) C467–C479.

[53] R.B. Figueira, C.J. Silva, E.V. Pereira, M.M. Salta, Alcohol-aminosilicate hybrid coatings for corrosion protection of galvanized steel in mortar, J. Electrochem. Soc. 161 (2014) C349–C362.

[54] B. Hirschorn, M.E. Orazem, B. Tribollet, V. Vivier, I. Frateur, M. Musiani, Determination of effective capacitance and film thickness from constant-phase-element parameters, Electrochim. Acta 55 (2010) 6218–6227, https://doi.org/10.1016/j.electacta.2009.10.065.

[55] S. Islama, H. Bakhtiar, M.B. Duralima, H.H.J.B. Sapingi, S. Riaz, S. Naseemb, N.B. Musaa, L. pik Suana, M. bin Abdullaha, Influence of organic pH dyes on the structural and optical characteristics of silica nanostructured matrix for fiber optic sensing, Sens. Actuators A: Phys. 282 (2018) 28–38, https://doi.org/10.1016/j.sna.2018.09.013.

[56] V. Bekiari, P. Lianos, U.L. Stangar, B. Orel, P. Judeinstein, Optimization of the intensity of luminescence emission from silica/poly(ethylene oxide) and silica/poly(propylene oxide) nanocomposite gels, Chem. Mater. 12 (2000) 3095–3099, https://doi.org/10.1021/cm0010598.

[57] E. Cordoncillo, F.J. Guaita, P. Escribano, C. Philippe, B. Viana, C. Sanchez, Blue emitting hybrid organic–inorganic materials, Opt. Mater. 18 (2001) 309–320, https://doi.org/10.1016/S0925-3467(01)00170-7.

[58] N.M. José, L.A.S. de Almeida Prado, M.A. Schiavon, S.U.A. Redondo, I.V.P. Yoshida, Partially pyrolyzed poly(dimethylsiloxane)-based networks: thermal characterization and evaluation of the gas permeability, J. Polym. Sci., Part B: Polym. Phys. 45 (2007) 299–309, https://doi.org/10.1002/polb.21053.

[59] L.A.S.A. De Prado, I.L. Torriani, I.V.P. Yoshida, Poly(n -alkylsilsesquioxane)s: synthesis, characterization, and modification with poly(dimethylsiloxane), J. Polym. Sci., Part A: Polym. Chem. 48 (2010) 1220–1229, https://doi.org/10.1002/pola.23885.

[60] R.B. Figueira, C.J.R. Silva, E.V. Pereira, Hybrid sol–gel coatings for corrosion protection of galvanized steel in simulated concrete pore solution, J. Coat. Technol. Res. 13 (2016) 355–373, https://doi.org/10.1007/s11998-015-9751-7.

[61] H.F.W. Taylor, C. Famy, K.L. Scrivener, Delayed ettringite formation, Cem. Concr. Res. 31 (2001) 683–693, https://doi.org/10.1016/S0008-8846(01)00466-5.

[62] Safety Data Sheet for Phenolphthalein, Phenolphthalein SDS. (2022). https://www.merckmillipore.com/PT/en/product/msds/MDA_CHEM-107233?ReferrerURL=https%3A%2F%2Fwww.bing.com%2F.

[63] Y.-S. Ho, Pseudo-Isotherms using a second order kinetic expression constant, Adsorption 10 (2004) 151–158, https://doi.org/10.1023/B:ADSO.0000039870.28835.09.

[64] C.T. Cesco, A.J.M. Valente, A.T. Paulino, Methylene blue release from chitosan/pectin and chitosan/DNA blend hydrogels, Pharmaceutics. 13 (2021) 842, https://doi.org/10.3390/pharmaceutics13060842.

[65] J. Crank, The mathematics of diffusion, 2d ed., Clarendon Press, Oxford, [Eng], 1975.

[66] D. Costa, A.J.M. Valente, M.G. Miguel, J. Queiroz, Gel Network Photodisruption: a New Strategy for the Codelivery of Plasmid DNA and Drugs, Langmuir 27 (2011) 13780–13789, https://doi.org/10.1021/la2026285.